Zeng *et al. Energy Mater* 2024;4:400029
DOI: 10.20517/energymater.2023.93

Energy Materials

Article

Open Access

Check for updates

Stable ultrathin lithium metal anode enabled by self-adapting electrochemical regulating strategy

Si-Yuan Zeng[1,#], Wen-Long Wang[1,#], Deyuan Li[2], Chunpeng Yang[2], Zi-Jian Zheng[1,*]

[1]Ministry of Education Key Laboratory for the Green Preparation and Application of Functional Materials, Hubei Key Laboratory of Polymer Materials, Hubei University, Wuhan 430062, Hubei, China.
[2]School of Chemical Engineering and Technology, Tianjin University, Tianjin 300072, China.
[#]Authors contributed equally.

[*]**Correspondence to:** Prof. Zi-Jian Zheng, College of Chemistry, Ministry of Education Key Laboratory for the Green Preparation and Application of Functional Materials, Hubei Key Laboratory of Polymer Materials, Hubei University, 368 Youyi Road, Wuhan 430062, Hubei, China. E-mail: zhengzj@hubu.edu.cn

How to cite this article: Zeng SY, Wang WL, Li D, Yang C, Zheng ZJ. Stable ultrathin lithium metal anode enabled by self-adapting electrochemical regulating strategy. *Energy Mater* 2024;4:400029. https://dx.doi.org/10.20517/energymater.2023.93

Received: 26 Nov 2023 **First Decision:** 2 Jan 2024 **Revised:** 22 Jan 2024 **Accepted:** 8 Feb 2024 **Published:** 8 Apr 2024

Academic Editor: Jiaqi Huang **Copy Editor:** Dong-Li Li **Production Editor:** Dong-Li Li

Abstract

Ultrathin lithium (Li) metal foils with controllable capacity could realize high-specific-energy batteries; however, the pulverization of Li metal foils due to its extreme volume change results in rapid active Li loss and capacity fading. Here, we report a strategy to stabilize ultrathin Li metal anode via *in-situ* transferring Li from ultrathin Li foil into a well-designed three-dimensional gradient host during a cycling process. A three-dimensional carbon fiber with gradient distribution of Ag nanoparticles is placed on the ultrathin Li foil in advance and acts as a Li reservoir, guiding Li deposition into its interior and thus alleviating the volume change of ultrathin Li foil anodes. Hence, a high reversibility of Li metal is achieved and Li pulverization is suppressed, which can be witnessed by a long cyclic life in the symmetric cells. The proposed method offers a versatile and facile approach for protecting ultrathin Li metal anodes, which will boost their commercial application process.

Keywords: Li metal anode, 3D scaffold, self-adapting, long lifespan, stability

INTRODUCTION

Metallic lithium (Li) is a potential anode material for rechargeable batteries due to its high theoretical specific capacity (3,860 mAh·g^{-1}) and low redox potential (-3.04 V *vs.* the standard hydrogen electrode)[1-4].

Ultrathin Li metal foils matching with commercial lithium transition metal oxide cathodes are expected to achieve high-specific-energy rechargeable batteries[5-8]. However, the high chemical reactivity of Li metal makes metallic Li spontaneously react with non-aqueous electrolytes to form solid electrolyte interphase (SEI) layers, contributing to low Li plating/stripping efficiency and low Li utilization rate[9-11]. In addition, because of the conversion reaction and the hostless Li plating/stripping characteristic, the Li metal anode suffers from infinite volume changes during cycling, which are highly responsible for the pulverization of Li metal, active Li loss, and the blocking of ionic transport[12,13].

Constructing a well-designed SEI layer on ultrathin Li foil has proved effective in suppressing Li/electrolyte interfacial parasitic reaction and alleviating Li dendrite penetration[14-18]. Thus, numerous artificial SEI layers, including organic layers[19-21], inorganic layers[22-24], and organic-inorganic hybrid layers[25,26], are designed and adopted to protect the ultrathin Li metal anodes. However, the constant volume fluctuation from the intrinsic hostless characteristic of Li metal anodes challenges the structure stability in the long running. Studies have shown that encapsulating active Li metal into a host is efficacious in addressing the volume change issue[27-29]. Therefore, various micro/nanostructured hosts have been widely studied, including three-dimensional (3D) Cu current collectors[30,31], reduced graphene oxide[32-35], carbon fibers[36-39], porous carbon granules[40-43], and so on. Combined with the high lithiophilic sites, the plating/stripping behaviors and the cycling performances of the composite metallic Li anode have seen great improvement. The common method that loads Li into 3D hosts can be clarified into electrochemical plating and melting strategy. The electrochemical pre-plating strategy can strictly control the amount of Li; however, this method is usually needed to assemble, disassemble and re-assemble the batteries, which is highly time-consuming and high-cost[44]. The melting strategy can avoid the complex processes, but the as-prepared composite anodes generally demonstrate a low Li utilization[45]. Therefore, it is imperative to explore a facile, highly efficient and inexpensive method to protect ultrathin Li metal anodes.

Herein, a self-adapting electrochemical regulating strategy, that is, *in-situ* self-migrating of Li metal from ultrathin Li foil into a well-designed 3D host by electrochemical cycling, is used to extend the cycling life of ultrathin Li anode. The key-enabling technique is to design a lithiophilic host with gradient distribution of Ag nanoparticles. Then, this well-designed host is directly placed on a commercial ultrathin Li metal foil. During the cycling process, Li metal gradually migrates into the prestaging host with the aid of Ag nanoparticles, nucleates on the Ag nanoparticles, and grows from bottom to up in the host, which helps stabilize the ultrathin Li anode volume and avoid internal short-circuit arising from the electrical connection of Li dendrite between Li anodes and cathodes [Scheme 1]. Hence, the hybrid Li anode featuring dendrite-free morphology demonstrates high reversibility and superior cycling performance. The hybrid Li anode also demonstrates its application potential by presenting a long lifespan of 180 cycles at a very low N/P ratio of 1.5 under a high cathode areal capacity in full cells.

EXPERIMENTAL

The absorbent cotton (AC) was pressed into thin sheets with a hot press under a pressure of 15 MPa at 100 °C. Then, the carbonized cotton AC was obtained by heat-treating at 1,200 °C for 2 h. The prepared conductive carbon cotton (CC) was then placed in a high vacuum thermal evaporation system to plate Ag nanoparticles via a vaporizing method to prepare a 3D host with gradient distribution of Ag nanoparticles (CC-Ag).

Materials characterizations

Field emission scanning electron microscopy (Sigma 500) was carried out to characterize the microscopic morphology of the electrode materials, while an Energy dispersive spectrometer (EDS) was combined to

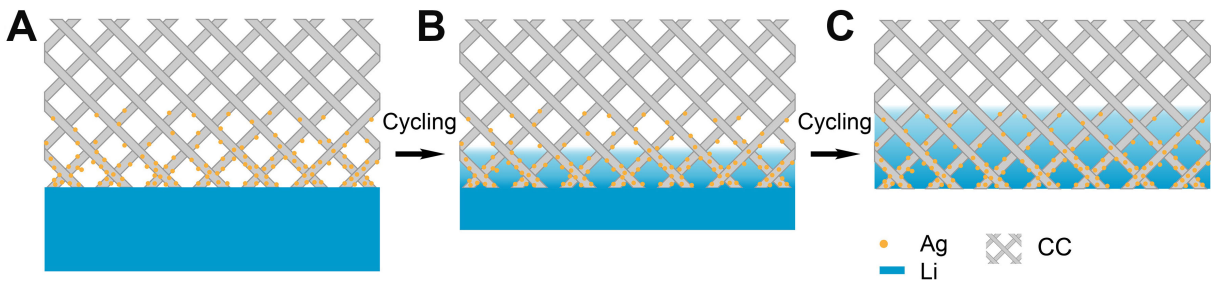

Scheme 1. Schematics of Li/CC-Ag hybrid anode before and after cycling. (A) CC-Ag stacked with ultrathin lithium before Li/CC-Ag cycle; (B) After a few turns of Li/CC-Ag cycles, ultrathin lithium is gradually transferred to CC-Ag; (C) Complete transfer of ultrathin lithium to CC-Ag after Li/CC-Ag cycles. CC: Carbon cotton.

qualitatively analyze the local elemental distribution of the samples. To observe the electrode morphology clearly, the cycled electrode was washed with 1,2-dimethoxyethane (DME) solvent repeatedly. The component of the CC and CC-Ag electrode was characterized by X-ray diffraction (XRD), which was conducted by using a Bruker D8 Advance with Cu Kα-rays (λ = 1.54 Å) as the target material at a current 40 mA and voltage 40 kV. The existence form of the Ag on the CC electrode was characterized by X-ray photoelectron spectroscopy (XPS).

Electrochemical tests

Electrochemical tests were performed by assembling CR2032 type coin cells in an argon-filled glove box and were tested on a NEWARE system. Celgard 2400 served as the separator, and 1 M LiTFSI/DOL-DME (V/V = 1:1) + 2 wt% $LiNO_3$ was adopted as the electrolyte. An ultrathin Li plated on the CC or CC-Ag denoted as Li/CC, Li/CC-Ag pairing with the bare Li foil was assembled into symmetric cells. $LiFePO_4$ (LFP) cathode, polyvinylidene fluoride binder, and conducting super P, at a weight ratio of 8:1:1, were ground to prepare the LFP cathode slurry. Full cells based on the Li foil, Li/CC, or Li/CC-Ag anodes and LFP cathode were assembled.

RESULTS AND DISCUSSION

A simple method, involving carbonization of natural cotton followed by thermal evaporation of Ag nanoparticles, was developed to prepare a 3D carbon host with gradient lithiophilicity (CC-Ag) [Figure 1A]. The CC derived from the carbonized cotton exhibits a 3D interconnected network distributed of C and N elements [Supplementary Figure 1]. After a thermal evaporation process, abundant nanoparticles with an average diameter of 50-60 nm are homogeneously distributed on the CC [Supplementary Figure 2]. The nanoparticles are identified as Ag element evidenced by the typical Ag characteristic peaks in the XRD patterns and XPS, as well as the signal of Ag in the EDS elemental mapping [Figure 1B, Supplementary Figures 2 and 3]. The Ag nanoparticles build a lithiophilic layer with an average thickness of about 30 μm, endowing a lithiophilic-lithiophobic gradient characteristic of the CC scaffold [Figure 1C and D]. The Ag nanoparticles enable improved electrical conductivity of 18.1 $S \cdot cm^{-1}$ for the CC-Ag, which is superior to that of 3.5 $S \cdot cm^{-1}$ for CC [Supplementary Figure 4].

Due to the inevitable parasitic reaction and large electrode volume change, ultrathin Li foil usually suffers from the obsession of pulverization and inactive Li gathering during long-term cycling. Putting a 3D host with lithiophilic gradient structure on the ultrathin Li is expected to realize the self-migration of Li metal from ultrathin Li foil into the host upon cycling and form 3D composite Li metal anodes and, therefore, address the above issues. The self-adapting regulating ability of the CC-Ag is elucidated by the schematic diagrams [Figure 2A and B] and the *ex-situ* scanning electron microscopy (SEM) images [Figure 2C-F].

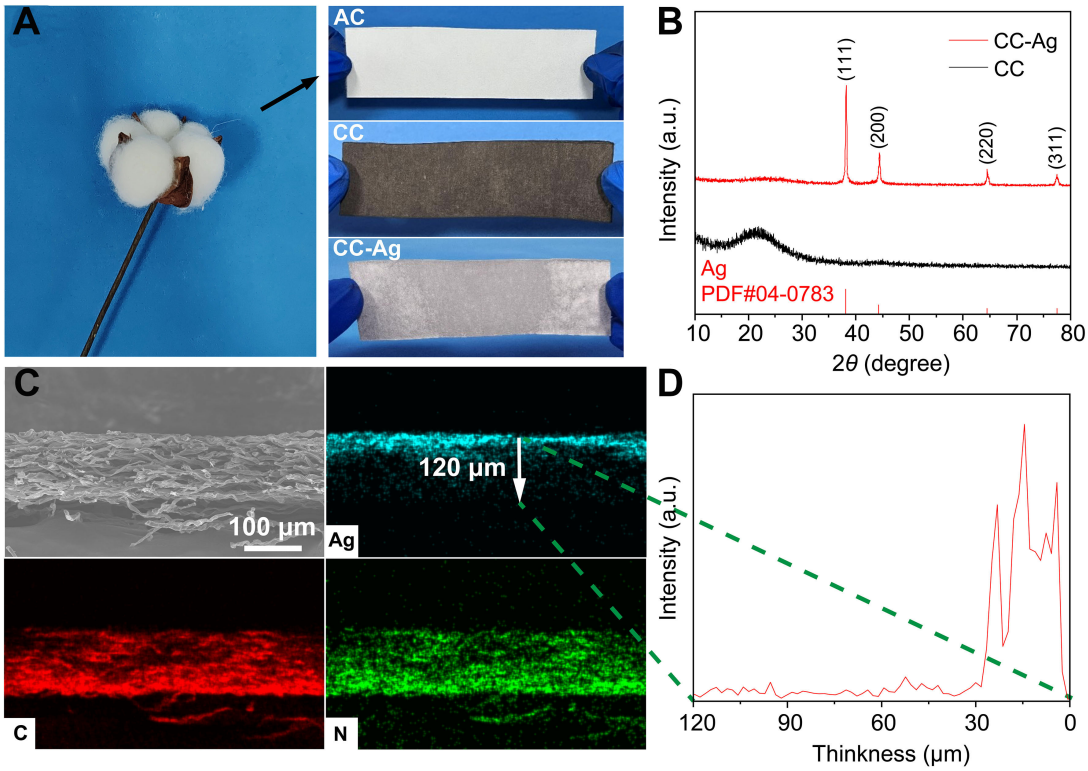

Figure 1. (A) Optical images of cotton, AC, CC, and CC-Ag; (B) XRD results of CC and CC-Ag; (C) SEM cross-sectional image of CC-Ag and corresponding elemental mappings; (D) Linear elemental mapping of Ag element along the CC-Ag. AC: Absorbent cotton; CC: carbon cotton; XRD: X-ray diffraction; SEM: scanning electron microscopy.

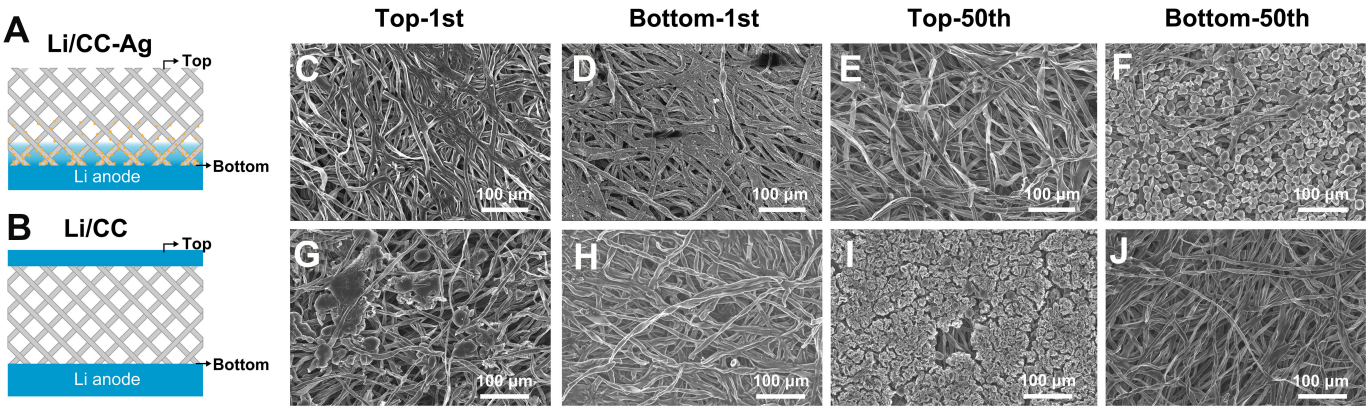

Figure 2. Schematic diagram of (A) Li/CC-Ag and (B) Li/CC during cycling; (C) Top and (D) bottom SEM images of Li/CC-Ag anode after the first cycle; (E) Top and (F) bottom SEM images of Li/CC-Ag anode after 50 cycles; (G) Top and (H) bottom SEM images of Li/CC anode after the first cycle; (I) Top and (J) bottom SEM images of Li/CC anode after 50 cycles. These electrodes were cycled at 0.5 mA·cm^{-2} with a capacity of 2 mAh·cm^{-2}. CC: Carbon cotton; SEM: scanning electron microscopy.

Prior to the morphological characterization, Li||Li symmetric cells were prepared by putting the CC-Ag electrode containing Ag side on the ultrathin Li foil while a Li foil serves as the counter electrode. Due to the good affinity of Ag to Li and the lithiophilic difference between the bottom and top of the CC, Li tends to deposit on the bottom of the CC-Ag [Figure 2C and D]. Upon the cycling, more Li can be observed on the

bottom of the CC-Ag, indicating ultrathin Li gradually self-migrates into the interconnected network of CC-Ag from bottom to up [Figure 2E and F, Supplementary Figure 5]. Due to the high porosity of the CC-Ag, the areal capacity around 8.1 mAh·cm^{-2} [Supplementary Figure 6] of an ultrathin Li anode can be well accommodated into the CC-Ag. For comparison, the Li morphological evolution on the bare CC without Ag was also investigated to demonstrate the importance of lithiophilic gradient structure in the Li self-inducing deposition. Due to the absence of lithiophilic gradient structure, the Li metal directly deposits on the surface of CC after the initial cycle [Figure 2G and H]. As the cycle goes on, Li metal continuously plates on the CC surface and gradually emerges into Li dendrites, increasing the risk of short circuits [Figure 2I and J].

The reversibility and electrochemical activity of Li from the ultrathin Li foil are verified by the electrochemical performances. The Li/CC-Ag delivers a high Li Coulombic efficiency of 99.5% at 0.5 mA·cm^{-2} with a capacity of 8 mAh·cm^{-2}, indicating a high Li reversibility can be achieved [Supplementary Figure 7]. In addition, the Li||Li symmetric cells were assembled to evaluate the Li/CC-Ag electrode stability. The Li||Li/CC-Ag symmetric cells present longer cycle life for over 2,000 h and lower polarization voltage of less than 20 mV at 0.5 mA·cm^{-2} with 2 mAh·cm^{-2} than those of Li||Li/CC (1,000 h/30 mV) and Li||Li cells (800 h/50 mV) [Figure 3A], confirming that the Li/CC-Ag has better cycling reversibility and volume stability. After cycling for 800 h, the Li/CC-Ag and Li/CC remain a typical plateau characteristic while the Li foil exhibits an arching voltage trace, indicating the interfacial mass transport of ultrathin Li is blocked by the generated dead Li [Figure 3B]. Electrochemical impedance spectrum (EIS) was further performed on the cycled Li/CC-Ag to evaluate the interfacial stability and charge transfer ability. The first semicircle at the high-frequency region is in connection with Li^+ transport through the SEI interfacial layer [Figure 3C]. The Li||Li/CC-Ag symmetric cells show smaller interfacial resistance, which is mainly due to the uniform Li morphology and suppressed Li/electrolyte interfacial side reactions. The second semicircle at the low-frequency region relates to the charge transfer resistance. The charge transfer resistance of Li||Li/CC-Ag symmetric cells is lower than that of Li||Li/CC-Ag symmetric cells, indicating the improved electronic conductivity and Li^+ transport ability of the Li/CC-Ag electrode. After 1,920 h (240th) cycling, the charge transfer resistance of the Li||Li/CC-Ag symmetric cells decreases from 2.6 to 1.5 Ω, which can be attributed to the generated mixed Li^+/e^- conductor of Li/CC-Ag anodes [Figure 3D]. Galvanostatic intermittent titration technique (GITT) test is adopted to characterize the transport kinetic differences for the two symmetric cells. The Li||Li/CC-Ag symmetric cells demonstrate lower overpotential than the Li||Li/CC symmetric cells, confirming faster mass transport kinetics related to the less accumulation of pulverized Li or dead Li for the Li/CC-Ag [Supplementary Figure 8].

Mossy Li or dendritic Li is easy to detach from the bulk Li foil and form electrically isolated dead Li at high areal capacity or current density. Hence, the symmetric cells were cycled at 1 mA·cm^{-2} with a capacity of 8 mAh·cm^{-2} per charge/discharge cycle. The Li/CC-Ag symmetric cells remain long cycling for more than 600 h without obvious overpotential increasement [Figure 3E], indicating the pulverization of Li is effectively alleviated by Li/CC-Ag. Increasing the current densities and deposition capacities, increasing overpotentials for the two types of symmetric cells are clearly observed in the voltage profiles. Wherein, the height of the voltage arcing regions for the Li/CC-Ag is lower than that of Li/CC, demonstrating the accumulation of dead Li is delayed by CC-Ag [Figure 3F].

Full cells in combination with a high areal capacity LFP cathode (> 1.7 mAh·cm^{-2}) and Li/CC-Ag or Li/CC anode were assembled to verify the application possibility of the self-transferring of Li metal from ultrathin Li foil into a 3D host. The Li/CC-Ag|LFP full cell anode delivers the highest reversible capacity of 148 mAh·g^{-1} with the minimum voltage overpotential at 0.5 C [Figure 4A]. After 250 cycles, the discharge

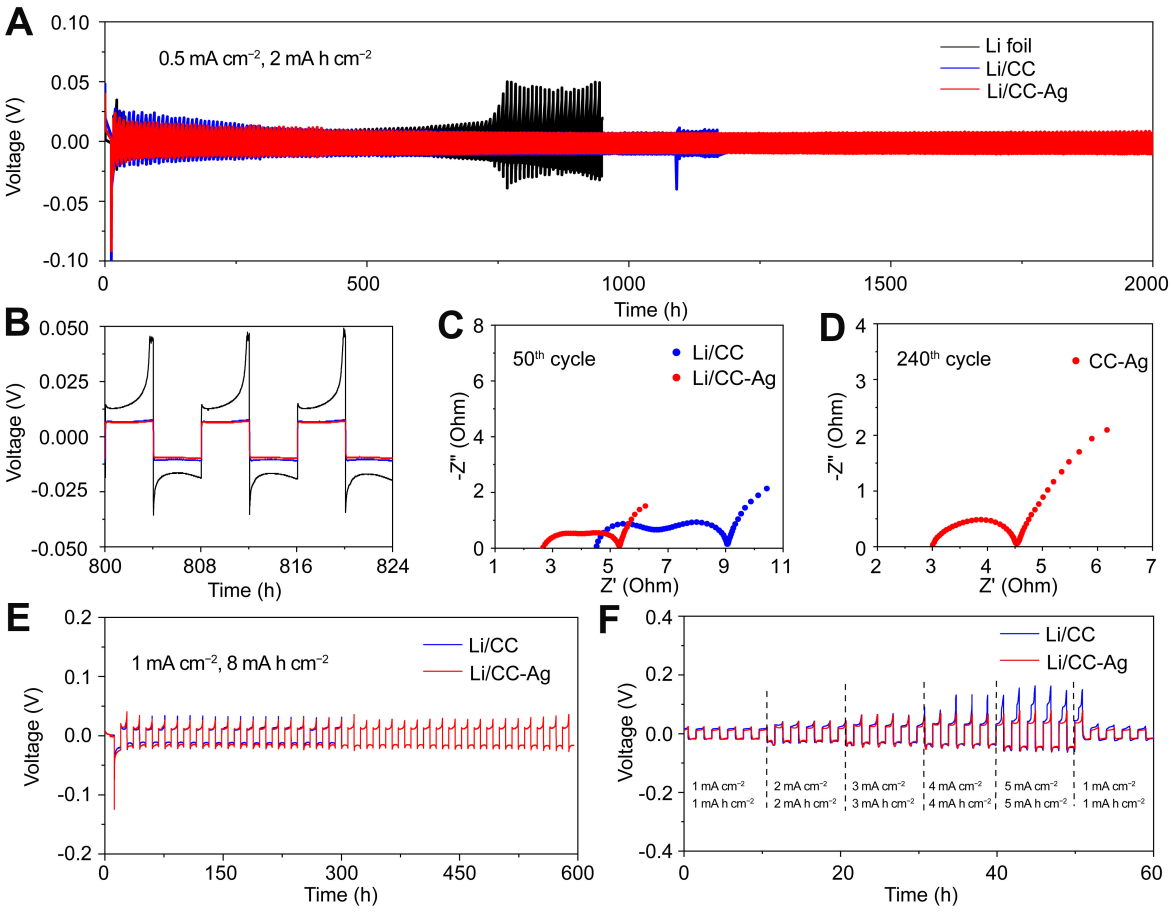

Figure 3. (A) Voltage *vs.* time of Li/CC-Ag, Li/CC and Li foil-based symmetric cells and (B) the enlarged polarization voltage comparison for the three electrodes; (C) Comparison of the EIS of the Li/CC-Ag and Li/CC symmetric cells; (D) EIS of the Li/CC-Ag symmetric cells after 240 cycles; (E) Voltage *vs.* time of Li/CC-Ag and Li/CC symmetric cells at 1 mA·cm^{-2} with a capacity of 8 mAh·cm^{-2}; (F) Voltage *vs.* time of Li/CC-Ag and Li/CC symmetric cells performed at increasing current densities and capacities. CC: Carbon cotton; EIS: electrochemical impedance spectrum.

capacity of the full cell with the Li/CC-Ag anode is maintained at 136 mAh·g^{-1}, which corresponds to a high-capacity retention of 92%. In comparison, the full cells with the Li/CC and Li foil anode exhibit rapid capacity decay [Figure 4B]. The superior transport kinetics of Li in the CC-Ag scaffold can also be seen from the smallest charge transfer resistance [Figure 4C]. The possible reason for the improved kinetics using the Li/CC-Ag anode is that the less accumulation of dead Li. Hence, further increasing the rate to 1.0 C [Figure 4D], the cell maintains a reversible capacity of 134 mAh·g^{-1} for 300 cycles with the Coulombic efficiency approaching 100% in each cycle. Upon increasing the areal capacity of the LFP cathode, the full cells pairing with Li/CC-Ag anode still demonstrate superior electrochemical performances. The full cells deliver high reversible capacities of 5.3 and 4.8 mAh·cm^{-2} at 0.1 and 0.5 C at a very low N/P ratio of 1.5, respectively, and maintain for 180 cycles without significant capacity attenuation [Figure 4E]. With further reducing the N/P ratio to 1.2, the full cells deliver a high reversible capacity of 5.1 mAh·cm^{-2} and 4.2 mAh·cm^{-2} at 0.1 and 0.5 C [Figure 4F]. Full cells were assembled by pairing the Li/CC-Ag anode with high-nickel $LiNi_{0.6}Mn_{0.2}Co_{0.2}O_2$ (NCM622) cathode to verify its application feasibility. As shown in Supplementary Figure 9, the full cell shows an initial capacity of 171.2 mAh·g^{-1} at 0.5 C and remains a reversible capacity of 162.9 mAh·g^{-1} after 200 cycles, corresponding to a high-capacity retention rate of 92.3%. The cell performances based on the Li/CC-Ag anode are competitive with reported cells using

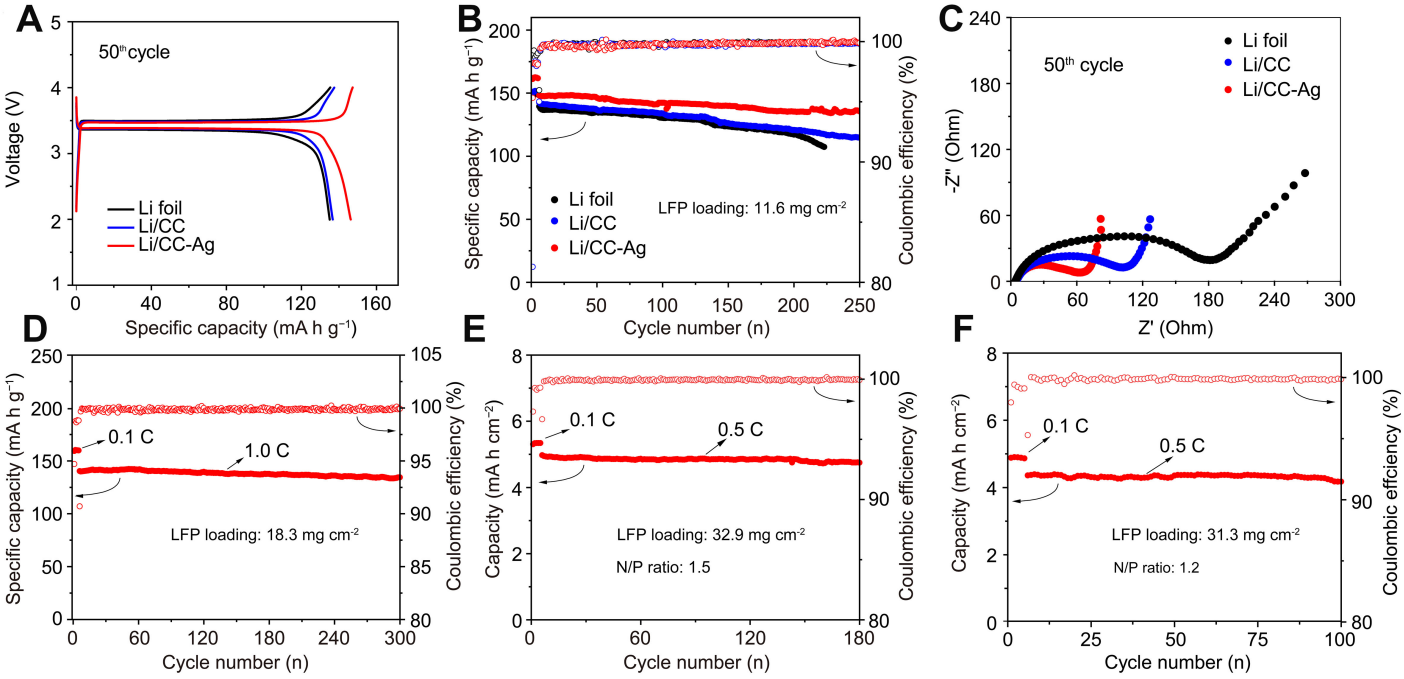

Figure 4. (A) Voltage *vs.* capacity of Li/CC-Ag||LFP, Li/CC||LFP, and Li foil||LFP full cells at 0.5 C after 50 cycles and (B) their long-time cycling of these three full cells; (C) The 50th Nyquist impedance plots of Li/CC-Ag||LFP and Li/CC||LFP full cells at 0.5 C; (D) Capacity *vs.* cycle number of LFP full cell with the Li/CC-Ag at 1.0 C; (E) Capacity *vs.* cycle number of the high capacity LFP full cell with the Li/CC-Ag at 0.5 C; (F) Capacity *vs.* cycle number of Li/CC-Ag||LFP full cell at a low N/P ratio at 0.5 C. CC: Carbon cotton; LFP: $LiFePO_4$.

composite Li anodes in the literature [Supplementary Table 1], demonstrating the application possibility of ultra-thin Li anode with the self-adapting strategy.

CONCLUSIONS

In conclusion, we reported a practical method to utilize ultrathin Li foil by directly placing Ag-modified 3D carbon fiber on its surface. The well-designed 3D carbon fiber features gradient lithiophilic sites. During electrochemical cycling, the Li resources gradually self-transferred into the 3D carbon fiber from bottom to up, ensuring the high reversibility and electrode volume stability. As a result, the hybrid anode containing ultrathin Li metal and 3D carbon fiber exhibits a Li utilization rate of about 83% and a long cycling performance of over 2,000 h. Full cell assembled by this hybrid anode delivers up to 180 stable cycles under a low N/P ratio (≤ 1.5). These results show good potential for the self-adapting electrochemical regulating strategy in prolonging the lifespan of ultrathin Li metal anode for high-specific-energy Li metal batteries.

DECLARATIONS

Authors' contributions

Data curation, formal analysis, investigation, writing - original draft: Zeng SY
Data curation, formal analysis, investigation: Wang WL
Writing - review and editing: Li D
Supervision, writing - review and editing: Yang C
Supervision, funding acquisition, writing - review and editing: Zheng ZJ

Availability of data and materials

The data supporting our work can be found in the Supplementary Materials.

Financial support and sponsorship
This work was supported by the National Natural Science Foundation of China (grant No. 22179036).

Conflicts of interest
All authors declared that there are no conflicts of interest.

Ethical approval and consent to participate
Not applicable.

Consent for publication
Not applicable.

REFERENCES
1. Lin D, Liu Y, Cui Y. Reviving the lithium metal anode for high-energy batteries. *Nat Nanotechnol* 2017;12:194-206. DOI PubMed
2. Zhang Y, Zuo T, Popovic J, et al. Towards better Li metal anodes: challenges and strategies. *Mater Today* 2020;33:56-74. DOI
3. Lu G, Nai J, Luan D, Tao X, Lou XWD. Surface engineering toward stable lithium metal anodes. *Sci Adv* 2023;9:eadf1550. DOI PubMed PMC
4. Zhang W, Zhang F, Liu S, et al. Regulating the reduction reaction pathways via manipulating the solvation shell and donor number of the solvent in Li-CO_2 chemistry. *Proc Natl Acad Sci U S A* 2023;120:e2219692120. DOI PubMed PMC
5. Shi P, Cheng XB, Li T, et al. Electrochemical diagram of an ultrathin lithium metal anode in pouch cells. *Adv Mater* 2019;31:e1902785. DOI PubMed
6. Chen H, Yang Y, Boyle DT, et al. Free-standing ultrathin lithium metal-graphene oxide host foils with controllable thickness for lithium batteries. *Nat Energy* 2021;6:790-8. DOI
7. Jin D, Roh Y, Jo T, Ryou M, Lee H, Lee YM. Robust cycling of ultrathin Li metal enabled by nitrate-preplanted Li powder composite. *Adv Energy Mater* 2021;11:2003769. DOI
8. Li T, Shi P, Zhang R, Liu H, Cheng X, Zhang Q. Dendrite-free sandwiched ultrathin lithium metal anode with even lithium plating and stripping behavior. *Nano Res* 2019;12:2224-9. DOI
9. Cheng XB, Zhang R, Zhao CZ, Zhang Q. Toward safe lithium metal anode in rechargeable batteries: a review. *Chem Rev* 2017;117:10403-73. DOI PubMed
10. Gao RM, Yang H, Wang CY, Ye H, Cao FF, Guo ZP. Fatigue-resistant interfacial layer for safe lithium metal batteries. *Angew Chem Int Ed Engl* 2021;60:25508-13. DOI PubMed
11. Cheng B, Zheng ZJ, Yin X. Recent progress on the air-stable battery materials for solid-state lithium metal batteries. *Adv Sci* 2024;11:e2307726. DOI PubMed PMC
12. Ye H, Zhang Y, Yin YX, Cao FF, Guo YG. An outlook on low-volume-change lithium metal anodes for long-life batteries. *ACS Cent Sci* 2020;6:661-71. DOI PubMed PMC
13. Wang C, Yang C, Zheng Z. Toward practical high-energy and high-power lithium battery anodes: present and future. *Adv Sci* 2022;9:e2105213. DOI PubMed PMC
14. Liu Y, Tao X, Wang Y, et al. Self-assembled monolayers direct a LiF-rich interphase toward long-life lithium metal batteries. *Science* 2022;375:739-45. DOI PubMed
15. Wu H, Jia H, Wang C, Zhang J, Xu W. Recent progress in understanding solid electrolyte interphase on lithium metal anodes. *Adv Energy Mater* 2021;11:2003092. DOI
16. Lee J, Choi SH, Qutaish H, et al. Structurally stabilized lithium-metal anode via surface chemistry engineering. *Energy Storage Mater* 2021;37:315-24. DOI
17. Li Q, Zhang J, Zeng Y, et al. Lithium reduction reaction for interfacial regulation of lithium metal anode. *Chem Commun* 2022;58:2597-611. DOI PubMed
18. Cheng Y, Wang Z, Chen J, et al. Catalytic chemistry derived artificial solid electrolyte interphase for stable lithium metal anodes working at 20 mA cm^{-2} and 20 mAh cm^{-2}. *Angew Chem Int Ed Engl* 2023;62:e202305723. DOI PubMed
19. Wang Y, Wang Z, Zhao L, et al. Lithium metal electrode with increased air stability and robust solid electrolyte interphase realized by silane coupling agent modification. *Adv Mater* 2021;33:e2008133. DOI PubMed
20. Kang D, Sardar S, Zhang R, et al. In-situ organic SEI layer for dendrite-free lithium metal anode. *Energy Storage Mater* 2020;27:69-77. DOI
21. Hou LP, Li Y, Li Z, et al. Electrolyte design for improving mechanical stability of solid electrolyte interphase in lithium-sulfur batteries. *Angew Chem Int Ed Engl* 2023;62:e202305466. DOI PubMed

22. Wang Z, Wang Y, Wu C, Pang WK, Mao J, Guo Z. Constructing nitrided interfaces for stabilizing Li metal electrodes in liquid electrolytes. *Chem Sci* 2021;12:8945-66. DOI PubMed PMC
23. Chen C, Liang Q, Wang G, Liu D, Xiong X. Grain-boundary-rich artificial SEI layer for high-rate lithium metal anodes. *Adv Funct Mater* 2022;32:2107249. DOI
24. Liu D, Xiong X, Liang Q, Wu X, Fu H. An inorganic-rich SEI induced by $LiNO_3$ additive for a stable lithium metal anode in carbonate electrolyte. *Chem Commun* 2021;57:9232-5. DOI PubMed
25. Xiao J, Zhai P, Wei Y, et al. In-situ formed protecting layer from organic/inorganic concrete for dendrite-free lithium metal anodes. *Nano Lett* 2020;20:3911-7. DOI PubMed
26. Zhang QK, Zhang XQ, Wan J, et al. Homogeneous and mechanically stable solid-electrolyte interphase enabled by trioxane-modulated electrolytes for lithium metal batteries. *Nat Energy* 2023;8:725-35. DOI
27. Feng Y, Zhang C, Li B, Xiong S, Song J. Low-volume-change, dendrite-free lithium metal anodes enabled by lithophilic 3D matrix with LiF-enriched surface. *J Mater Chem A* 2019;7:6090-8. DOI
28. Zheng ZJ, Su Q, Zhang Q, et al. Low volume change composite lithium metal anodes. *Nano Energy* 2019;64:103910. DOI
29. Jiang Q, Xiong P, Liu J, et al. A redox-active 2D metal-organic framework for efficient lithium storage with extraordinary high capacity. *Angew Chem Int Ed Engl* 2020;59:5273-7. DOI PubMed
30. Ye H, Zheng ZJ, Yao HR, et al. Guiding uniform Li plating/stripping through lithium-aluminum alloying medium for long-life Li metal batteries. *Angew Chem Int Ed Engl* 2019;58:1094-9. DOI PubMed
31. Chen J, Zhao J, Lei L, et al. Dynamic intelligent Cu current collectors for ultrastable lithium metal anodes. *Nano Lett* 2020;20:3403-10. DOI PubMed
32. Yang T, Li L, Wu F, Chen R. A soft lithiophilic graphene aerogel for stable lithium metal anode. *Adv Funct Mater* 2020;30:2002013. DOI
33. Liu S, Wang A, Li Q, et al. Crumpled graphene balls stabilized dendrite-free lithium metal anodes. *Joule* 2018;2:184-93. DOI
34. Feng X, Wu H, Gao B, Świętosławski M, He X, Zhang Q. Lithiophilic N-doped carbon bowls induced Li deposition in layered graphene film for advanced lithium metal batteries. *Nano Res* 2022;15:352-60. DOI
35. Xiong P, Yin H, Chen Z, et al. Thiourea-based polyimide/RGO composite cathode: a comprehensive study of storage mechanism with alkali metal ions. *Sci China Mater* 2020;63:1929-38. DOI
36. Zeng SY, Wang CY, Yang C, Zheng ZJ. Limited lithium loading promises improved lithium-metal anodes in interface-modified 3D matrixes. *ACS Appl Mater Interfaces* 2022;14:41065-71. DOI PubMed
37. Lee Y, Cho K, Lee S, et al. Construction of hierarchical surface on carbon fiber paper for lithium metal batteries with superior stability. *Adv Energy Mater* 2023;13:2203770. DOI
38. Chen H, Li M, Li C, et al. Electrospun carbon nanofibers for lithium metal anodes: Progress and perspectives. *Chin Chem Lett* 2022;33:141-52. DOI
39. Lu Q, Jie Y, Meng X, et al. Carbon materials for stable Li metal anodes: challenges, solutions, and outlook. *Carbon Energy* 2021;3:957-75. DOI
40. Yuan H, Nai J, Tian H, et al. An ultrastable lithium metal anode enabled by designed metal fluoride spansules. *Sci Adv* 2020;6:eaaz3112. DOI PubMed PMC
41. Huang W, Liu S, Yu R, Zhou L, Liu Z, Mai L. Single-atom lithiophilic sites confined within ordered porous carbon for ultrastable lithium metal anodes. *Energy Environ Mater* 2023;6:e12466. DOI
42. Lu C, Tian M, Wei C, Zhou J, Rümmeli MH, Yang R. Synergized N, P dual-doped 3D carbon host derived from filter paper for durable lithium metal anodes. *J Colloid Interface Sci* 2023;632:1-10. DOI PubMed
43. Feng YS, Li YN, Wang P, Guo ZP, Cao FF, Ye H. Work-function-induced interfacial electron/ion transport in carbon hosts toward dendrite-free lithium metal anodes. *Angew Chem Int Ed Engl* 2023;62:e202310132. DOI PubMed
44. Zheng ZJ, Ye H, Guo ZP. Recent progress in designing stable composite lithium anodes with improved wettability. *Adv Sci* 2020;7:2002212. DOI PubMed PMC
45. Li L, Li Y, Cao F, Ye H. Lithiophilic interface guided transient infiltration of molten lithium for stable 3D composite lithium anodes. *Nano Res* 2023;16:8297-303. DOI